Clin Neuroradiol (2015) 25:349–360
DOI 10.1007/s00062-015-0383-1

REVIEW ARTICLE

Clinical Applications of Cine Balanced Steady-State Free Precession MRI for the Evaluation of the Subarachnoid Spaces

A.E. Li · M.D. Wilkinson · K.M. McGrillen · M.A. Stoodley · J.S. Magnussen

Received: 7 January 2015 / Accepted: 26 February 2015 / Published online: 9 April 2015

Abstract The purpose of this article is to review the physiology of normal brain and spinal cord motion in the subarachnoid space, principles of cine balanced steady-state free precession (bSSFP) magnetic resonance imaging (MRI), clinical applications, and the pitfalls encountered with this technique.

The brain and spinal cord are dynamic structures that move with each heartbeat due to transmitted arterial pulse waves. Conventional MRI sequences do not allow anatomic evaluation of the pulsatile movement of the neural structures in the subarachnoid space due to limitations in temporal resolution. Cine bSSFP MRI uses cardiac gating to evaluate dynamically the brain and spinal cord with high contrast and temporal resolution.

Cine bSSFP can be used in the evaluation of idiopathic syringomyelia to assess an underlying treatable cause, including arachnoid bands, which are usually not well visualized with conventional MR sequences due to motion artifact. This MRI technique is also useful in the evaluation of intraspinal and intracranial arachnoid cysts and the degree of mass effect on the cord. Other applications include preoperative and postoperative evaluation of Chiari I malformation and the evaluation of lateral ventricular asymmetry. The major limitation of cine bSSFP is the presence of banding artifacts, which can be reduced by shimming and modifying other scan parameters.

Keywords Balanced steady-state free precession · Magnetic resonance imaging (MRI) · Syringomyelia · Arachnoid adhesions · Arnold–Chiari Malformation · Cerebrospinal fluid (CSF)

Electronic supplementary material The online version of this article (doi: 10.1007/s00062-015-0383-1) contains supplementary material, which is available to authorized users.

A.E. Li, MBBS, MMed, FRANZCR (✉) ·
M.D. Wilkinson, MBChB, BMedSci, FRANZCR ·
K.M. McGrillen, BAppSc, MBBS, FRANZCR ·
J.S. Magnussen, MBBS, PhD, FRANZCR
Radiology Department, Australian School of Advanced Medicine,
Ground Floor, Macquarie University Hospital,
3 Technology Place, Macquarie University,
2109 Sydney, New South Wales, Australia
e-mail: angela.li.rad@gmail.com

M.D. Wilkinson, MBChB, BMedSci, FRANZCR
e-mail: mcwilkinson@internode.on.net

K.M. McGrillen, BAppSc, MBBS, FRANZCR
e-mail: kymcgrillen@gmail.com

J.S. Magnussen, MBBS, PhD, FRANZCR
e-mail: johnm@scan.com.au

M.A. Stoodley, MBBS, PhD, FRACS
Neurosurgery Unit, Australian School of Advanced Medicine,
Macquarie University,
Sydney, Australia
e-mail: marcus@teamneuro.com

Introduction

Conventional anatomic imaging of the brain assumes it to be a largely static structure, with movement only occurring in blood vessels and cerebrospinal fluid (CSF). Routine magnetic resonance imaging (MRI) sequences of the brain and spinal cord are aimed at improving spatial and contrast resolution, often at the expense of temporal resolution.

Static balanced steady-state free precession (bSSFP) MRI is widely used in the evaluation of neural structures within the intracranial CSF, due to the high signal-to-noise ratio (SNR), contrast resolution, spatial resolution, and the ability to acquire contiguous blocks of data. However, rely-

ing on static techniques for diagnosis ignores the dynamics of the neural structures within the subarachnoid space: the brain and spinal cord move in synchrony with each arterial pulse wave.

Cine bSSFP is an MRI technique that uses retrospective cardiac gating to dynamically evaluate the brain and spinal cord, thereby providing high contrast and temporal resolution. Standard static MRI sequences of the brain and spinal cord are limited by temporal resolution leading to motion-related blurring of nonstatic structures. Cine bSSFP has superior temporal resolution, virtually eliminating movement artifact. At our institution, cine bSSFP has a temporal resolution of approximately 45 ms compared with 2500–5000 ms in conventional static T2-weighted (T2W) sequences.

Cine bSSFP MRI has been used in the diagnosis of arachnoid membranes in the subarachnoid space, which were not visible on conventional T2W sequences due to pulsatile motion of the structures in the spinal canal. Gottschalk et al. [1] reported a case of syringomyelia, in which preoperative cine bSSFP MRI demonstrated arachnoid membranes in the dorsal subarachnoid space, the presence of which was surgically confirmed when the patient underwent microsurgical lysis. Cousins and Haughton [2] used cine bSSFP to study the degree of motion of the cerebellar tonsils in the foramen magnum and found that there was 0.57-mm biphasic tonsillar displacement in patients with Chiari I malformation, compared with 0.43 mm in controls. The movement of the pulsatile neural structures including the lamina terminalis has also been studied with cine bSSFP [3].

Cine bSSFP has been used elsewhere in the body, most notably in cardiac MRI. The high contrast between blood and myocardial or vessel wall makes it effective in the assessment of cardiac wall motion, ventricular function, and the cardiac valves [4]. Cine bSSFP has also been used in the dynamic evaluation of the pelvic floor, with images acquired at rest, during sphincter contraction, straining, and defecation [5]. Cine SSFP MRI technique has also been used with MR enterography to identify small bowel strictures and lesions, and evaluate intestinal motility [6].

In this article, we review normal brain motion, the physics of cine bSSFP, clinical applications, artifacts, and pitfalls.

Normal Dynamics of the Brain and CSF

The brain is not a static structure as may appear on standard MRI sequences. Brain motion is pulsatile, consisting of a single displacement in systole, followed by a gradual return to the normal position in diastole [7]. Several theories have been hypothesized for the physiology of pulsatile brain motion and CSF flow with the cardiac cycle, based on measured velocities demonstrated on phase-contrast MRI. The Monro–Kellie hypothesis states that the cranium has a fixed volume. The sum of the brain, blood (arteries and veins), and CSF volume is constant, and an increase in one component will cause a decrease in at least one of the other two components [8].

With each cardiac cycle, in early systole, there is an arterial pulsation with expansion of the intracranial arteries, leading to capillary dilatation. This causes expansion of the brain with caudal displacement of the central structures such as the diencephalon, brainstem, and cerebellar tonsils [9]. The normal degree of brain displacement is approximately 0.4 mm for the cerebellar tonsils, and 0.1–0.2 mm for the brainstem and other posterior fossa structures [2, 9] (Fig. 1). This is balanced by simultaneous cephalic motion of the more peripheral structures such as the cerebral hemispheres and posterior cerebellum [9].

The caudal motion of the brainstem is a rapid piston-like motion, causing displacement of CSF from the foramen magnum into the spinal subarachnoid space [10]. The CSF pulse wave then propagates through the spinal canal [10, 11]. The cervical cord also moves caudally with movement of the brainstem [9]. This expansion of the brain compresses the lateral ventricles, promoting CSF flow through the foramen of Monro and cerebral aqueduct. In diastole, there is a gradual return to the brain to its neutral position [7]. The overall direction of CSF flow is caudal in systole and cranial in diastole [11].

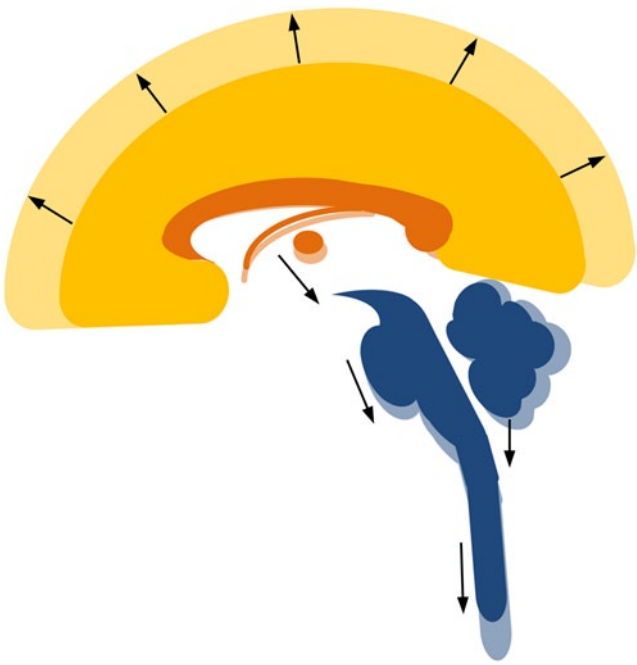

Fig. 1 The diagram depicts normal brain motion in systole. The arterial pulsation leads to expansion of intracranial arteries and capillaries. This causes expansion of the brain, with caudal motion of central structures, including the diencephalon, brainstem, and cerebellar tonsils. Conversely, the cerebral hemispheres demonstrate cranial motion

Table 1 Manufacturer names for balanced steady-state free precession sequences

Acronym	Full name	Manufacturer
bFFE	*B*alanced *F*ast *F*ield *E*cho	Philips Healthcare, Best/ Eindhoven, The Netherlands
TrueFISP	*T*rue *F*ast *I*maging with *S*teady-State *P*recession	Siemens Healthcare, Erlangen, Germany
FIESTA	*F*ast *I*maging *E*mploying *S*teady State *A*cquisition	GE Healthcare, Waukesha, Wisconsin, United States

Physics and Basic Principles of Cine bSSFP

bSSFP MRI is variously known as FIESTA, TrueFISP, and balanced FFE depending on the equipment manufacturer (Table 1).

Steady State

Steady-state free precession sequences are fast gradient acquisitions in which longitudinal and transverse magnetizations are kept constant from one time to repetition (TR) to another TR. The steady state is achieved by the use of a low flip angle (α) and a very short TR, shorter than the T2 relaxation times of the tissue such that $TR << T2 \leq T1$ [12].

A rapid succession of radiofrequency (RF) pulses is applied, preventing the magnetization from returning to the equilibrium state M_0. After a few hundred TR periods, a steady state or dynamic equilibrium is achieved in which the magnetization is unchanging over time, from one TR to another TR [12].

Balanced SSFP

Balanced SSFP refers to the use of balanced gradients in all three axes (slice selection, phase encoding, and readout) [4]. Dephasing caused by each applied gradient is compensated or balanced by applying a gradient of opposite polarity, to keep the gradient moment constant, with a net zero area over one TR (Fig. 2) [12]. This results in the sequence being relatively insensitive to motion. Furthermore, phase alternation of the RF pulse flip angle α by 180° (−α) occurs within a single TR [13].

Balanced SSFP uses both free induction decay and spin-echo components for image formation, the former of which contains mixed T1 and T2* weighting, and the latter which is strongly T2W with little T2*W [4]. Contrast in bSSFP is determined mainly by the T2/T1 ratio of tissue [12]. Tissues such as CSF have a high T2/T1 ratio, which results in high contrast between CSF and the brain and spinal cord [14, 15]. Static steady-state precession MRI has been used to obtain static 3D myelographic-like images of the cervical spine, with high SNR and high contrast between CSF and the spinal cord. SNR is high, as the transverse magnetization is generated by multiple TR combined. Increased SNR allows the use of a higher bandwidth, with shorter time to echo (TE) and TR, minimizing acquisition time [16].

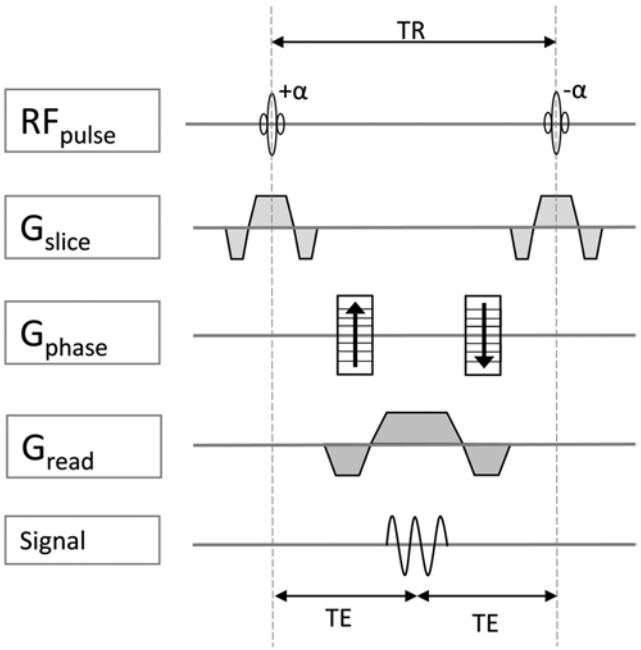

Fig. 2 MRI pulse sequence diagram for balanced steady-state free precession MRI. Gradients (*G*) are balanced in all three directions (slice selection, phase encoding, and readout). Over one repetition period (*TR*), the sum of positive gradients equals the sum of negative gradients with a net area of zero. There is no net dephasing of magnetization, which results in the sequence being relatively insensitive to motion. The radiofrequency (*RF*) pulse flip angle (*α*) undergoes 180° phase alternation with each TR. *TR* time to repetition, *TE* time to echo. (Modified and reprinted with permission, from Carr et al. [13])

Cardiac Gating for Cine Imaging

Cardiac gating is achieved by the use of an electrocardiogram (ECG) signal or recording a pulse oximetry trace. Data for a single slice are acquired at multiple points over the cardiac cycle, which are called cardiac phases [16]. The data for each cardiac phase is set to generate a single image corresponding to that cardiac phase. The images for all the cardiac phases are viewed sequentially in a cine loop. The number of phases and the heart rate determine the temporal resolution. For example, an acquisition with 20 cardiac phases and a heart rate of 72 beats/min results in a temporal resolution of 41.7 ms.

MRI Protocol

The MRI protocol at our institution is as follows: 3.0-T scanner (Siemens Verio) with a 32-channel head coil. Localizer images, T1W and T2W sequences of the brain, and cervical

spine are acquired in addition to phase-contrast sequences. These sequences are used to assess the best plane for cine bSSFP, which in most cases is a midline sagittal slice centered on the foramen magnum (for Chiari malformation) or at the level of spinal cord pathology. Additional cine bSSFP sequences can be obtained in the axial or coronal plane to further delineate pathology.

Peripheral pulse oximetry is used for cardiac synchronization, with 20 cardiac phases, segments set of 10–12, TE of 1.9 ms, TR of 41.7/20 = 2.1 ms, flip angle of 35–55°, field of view of 158 mm, bandwidth of 916 Hz, and in-plane resolution of 0.5 × 0.9 mm with a slice thickness of 3 mm. A cardiac shim protocol is performed prior to the scan to reduce banding artifact (see "Pitfalls and Artifacts" section). For studies of the spinal cord, a body surface coil is used. Peripheral cardiac synchronization with pulse oximetry is used, as opposed to ECG synchronization, due to its relative simplicity and without apparent compromise in diagnostic image quality. Total image acquisition time for this sequence is approximately 4.5 min.

Clinical Applications

The following clinical applications of cine bSSFP in studying the motion of neural structures in the subarachnoid space will be discussed: idiopathic syringomyelia, spinal intradural arachnoid cyst, lateral ventricular asymmetry, Chiari I malformation preoperative and postoperative evaluation, and other applications.

Idiopathic Syringomyelia

Syringomyelia refers to the formation of a cavity in the spinal cord. The syrinx may be associated with Chiari malformation, tumor, trauma, infection, or be "idiopathic," where no underlying cause has been demonstrated. A proportion of presumed idiopathic syringomyelia cases are thought to be due to the obstruction of CSF flow around the spinal cord, which may be due to underlying arachnopathies including arachnoid membranes or arachnoid cysts [17].

Microsurgical lysis is the treatment of choice for patients with symptomatic syringomyelia due to arachnoid adhesions. Identification of arachnoid membranes or adhesions is essential in the process of selecting patients for surgery.

Arachnoid membranes are usually not well seen on standard static T2 sequences due to motion blur with each CSF pulsation. High-resolution cine bSSFP allows visualization of arachnoid membranes and adhesions. Arachnoid adhesions appear as a thin transverse or obliquely oriented hypointense band between the spinal cord and dura. These bands generally move in synchrony with the spinal cord (Fig. 3; Movies 2 and 3).

Phase-contrast MRI can be utilized to detect the level of CSF flow obstruction, which is inferred by the absence of CSF pulsations [18] or by flow disturbance (Fig. 4d). The use of phase-contrast MRI alone is limited, as this technique relies on detection of flow abnormalities and assumptions about sites of obstruction and does not allow visualization of arachnoid membranes. Phase-contrast MRI can be performed in conjunction with bSSFP to evaluate which arachnoid bands cause CSF flow obstruction. Using both sequences allows the evaluation of the anatomy and dynamic significance of these arachnoid bands.

Spinal Intradural Arachnoid Cyst

Spinal arachnoid cysts are usually CSF-containing spaces lined by arachnoid mater and can be intradural or extradural in location. These may be primary lesions that are congenital or idiopathic. Primary intradural arachnoid cysts are usually located in the midline dorsally, arising from the septum posticum, which is a membranous partition in the dorsal spinal subarachnoid space in the thoracic region [19]. Secondary intraspinal arachnoid cysts are thought to arise from dural tears or adhesions related to previous trauma, inflammation, or hemorrhage, although the pathogenesis is debatable [20, 21]. Secondary arachnoid cysts can arise dorsally, ventrally, or laterally. Overall, the most common site for intraspinal arachnoid cysts is dorsal to the thoracic cord [21, 22].

Intradural arachnoid cysts may communicate with the subarachnoid space via a narrow neck and are then called arachnoid diverticula [21]. These cysts can enlarge due to a one-way valve effect, and cause spinal cord compression [20]. Other arachnoid cysts become walled off and are separate from the subarachnoid space.

These have been traditionally diagnosed by myelography, computed tomography myelography, or conventional MRI sequences [22, 23]. With myelographic techniques, the arachnoid cyst can be seen to fill with contrast medium if there is a communication between the cyst and the subarachnoid space. The drawback of myelography is the invasive nature of the technique. The presence of arachnoid cysts can be diagnosed on conventional MRI sequences if the cyst walls are visible, or may be inferred by the mass effect on the spinal cord. Phase-contrast MRI may demonstrate abnormal flow around the cyst, or dynamic spinal cord compression by the cyst, although anatomical details of the cyst are not delineated [24].

Intradural arachnoid cysts can be diagnosed with cine bSSFP, by visualization of the cyst walls, which appear as fine septa moving in synchrony with the spinal cord or with the transmitted CSF pulse wave (Figs. 4, 5, and 6; Movies 4–8). In addition, this technique provides high-resolution, dynamic assessment of the associated mass effect of intradural cystic structures on the spinal cord (Fig. 7; Movie 9).

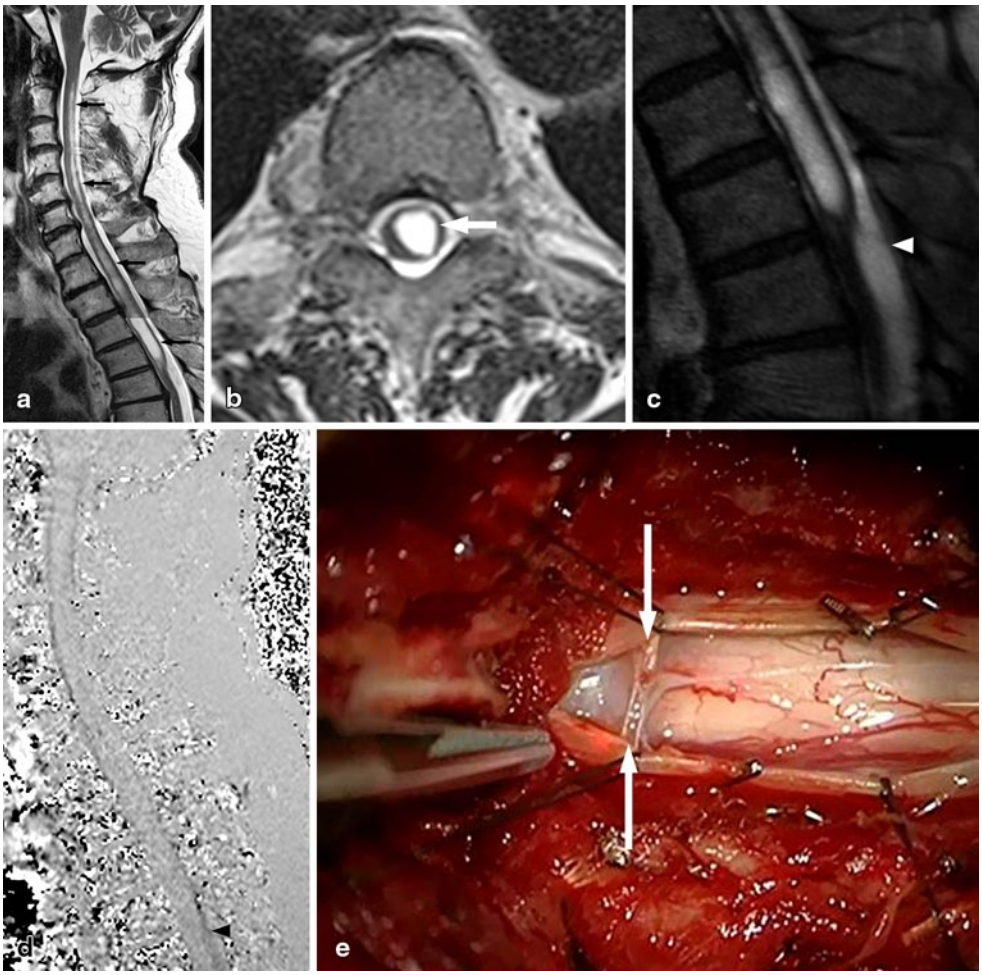

Fig. 3 Presumed idiopathic syringomyelia in a 63-year-old man with a long cervicothoracic syrinx, the etiology of which was initially unknown. **a** Sagittal T2-weighted (T2W) image demonstrates a long syrinx from the C2 to T4/5 level (*black arrows*). **b** Axial T2W image shows expansion of the spinal cord due to the syrinx (*white arrow*). **c** Single still image from cine bSSFP MRI shows a subtle linear hypointense band (*white arrowhead*). **d** Phase-contrast MRI demonstrates slightly disturbed, but still present, flow inferior to the known posterior arachnoid membrane at the T4/5 level (*white arrow*). **e** Intraoperative photo demonstrates an arachnoid band dorsal to the spinal cord (*white arrows*) corresponding to the band seen on MRI. See Movies 2 and 3 for corresponding cine bSSFP sequence and intraoperative video.

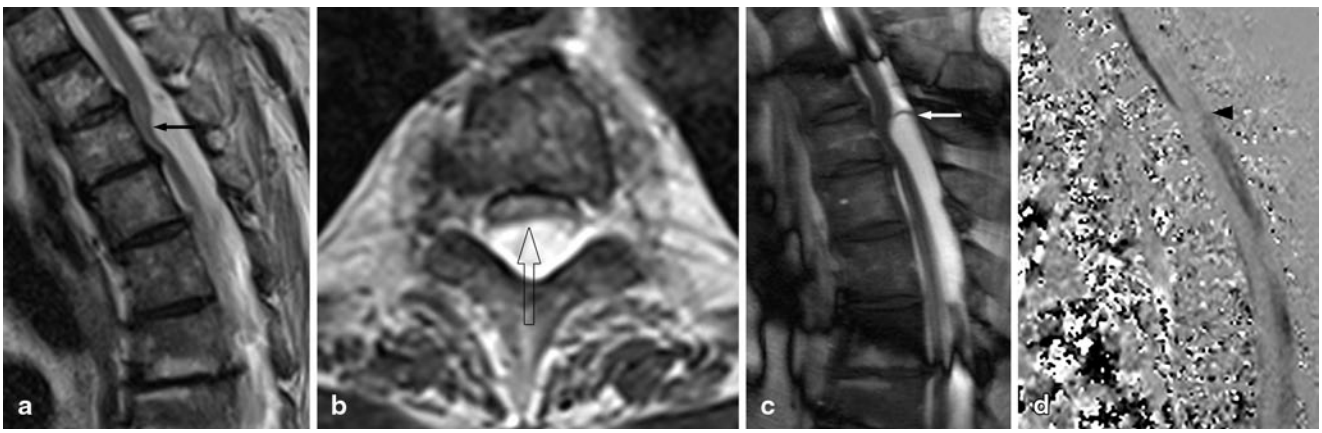

Fig. 4 An 80-year-old woman with sensory symptoms. The provisional diagnosis was thoracic cord herniation or an arachnoid cyst based on static MRI imaging. Sagittal (**a**) and axial (**b**) static T2W image shows focal anterior displacement of the spinal cord at T2/3 (*black arrow*). There is flattening of the spinal cord, with cord signal hyperintensity (*open arrow*). No arachnoid membrane is seen. **c** Still image frame from cine bSSFP MRI demonstrates the superior wall of an arachnoid cyst (*white arrow*), excluding the diagnosis of idiopathic cord herniation. **d** Phase-contrast MRI demonstrates prominent flow signal inferior to the arachnoid cyst wall at the T3 level, with disruption of flow at the level of the cyst wall (*black arrowhead*). Prominent flow signal within the cyst suggests communication with the CSF space. See Movie 4 for corresponding cine bSSFP sequence.

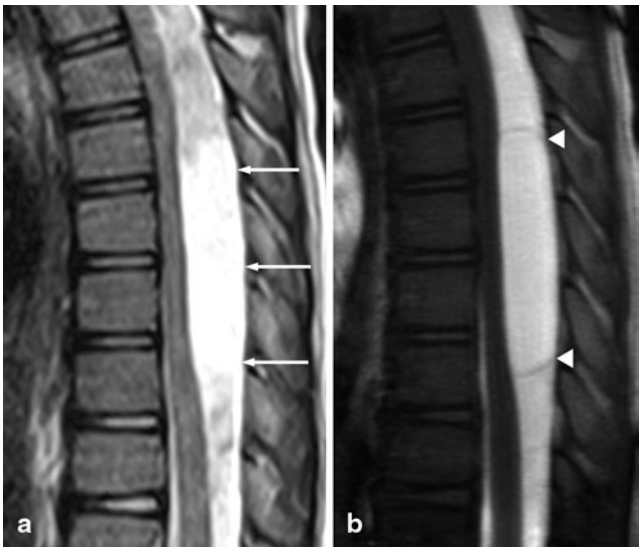

Fig. 5 A 9-year-old girl with large spinal intradural arachnoid cyst. **a** Sagittal T2W image shows a large CSF space dorsal to thoracic cord (*arrows*) with displacement of spinal cord anteriorly, suggestive of an arachnoid cyst. **b** Still image from cine bSSFP shows the superior and inferior cyst walls (*white arrowheads*). See Movies 5 and 6 for corresponding cine bSSFP sequence.

It is unlikely that cine bSSFP alone could differentiate an arachnoid cyst that communicates with the CSF space from one that does not, unless the plane of imaging included an obvious defect in the cyst wall. Phase-contrast cine MRI CSF jets have been described in communicating intracranial arachnoid cysts [25], and the larger cysts in our sample group all appear to demonstrate at least some degree of internal CSF flow on phase-contrast imaging (Movie 5). As the dynamic bSSFP sequences show (Movies 2, 4, and 7), the cyst walls and arachnoid membranes are often mobile in their own right, inducing adjacent fluid motion and potentially phase-contrast signal. It is not yet certain how these factors interrelate, given our small current sample size.

Lateral Ventricular Asymmetry

The finding of asymmetric lateral ventricles, with deviation of the septum pellucidum, is not uncommon. While the appearance may represent a normal anatomical variant, it is important to exclude an underlying intracranial cyst causing ventricular obstruction.

Intracranial cysts can have a similar appearance on imaging, although are histologically diverse, comprising arachnoid, ependymal, colloid, epidermoid, dermoid, neuroglial, or choroid plexus cysts [26]. Ependymal cysts develop as a result of sequestration of neuroectoderm during embryonic development [27]. These are thin-walled cysts lined by ependymal cells, which secrete the serous fluid into the cyst. The most common location is the lateral ventricles.

Intraventricular arachnoid cysts are rare with few reported cases in the literature [28, 29]. The more common extraventricular arachnoid cysts are thought to develop due to abnormal splitting and duplication of the arachnoid during embryonic development [29]. However, the ventricles do not normally contain arachnoid mater. It has been postulated that intraventricular arachnoid cysts arise from the vascular mesenchyme or by extension of an arachnoid cyst from the subarachnoid space into the lateral ventricles via the choroidal fissure [30, 31].

On MRI, intraventricular cysts appear as well-defined CSF signal intensity cysts with thin nonenhancing walls. The containing ventricle may appear enlarged. However, the cyst walls can be too fine to be seen on static MRI sequences due to normal motion of the brain, which blurs the cyst membranes. Cine bSSFP has the advantage of being able to resolve the fine cyst membranes to confirm the presence of a cyst. Phase-contrast MRI can be used to infer the presence of the cyst by demonstration of lack of flow in the region of the cyst, although the cyst walls are not actually seen. Conversely, lack of visualization of membranes sug-

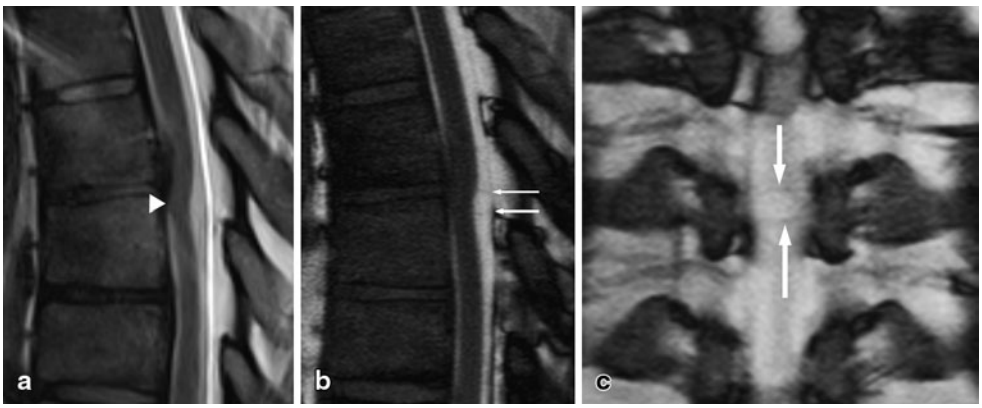

Fig. 6 Subtle case of intradural arachnoid cyst in a 35-year-old man. **a** Sagittal static T2W image shows focal anterior displacement of the spinal cord at T6/7 (*white arrowhead*). The differential diagnosis was initially idiopathic cord herniation or an arachnoid cyst. No cyst walls are visible. Still images from sagittal (**b**) and coronal (**c**) cine bSSFP sequence demonstrate a small arachnoid cyst dorsal to the spinal cord. The superior and inferior cyst walls (*white arrows*) are visible. See Movies 7 and 8 for corresponding cine bSSFP sequence.

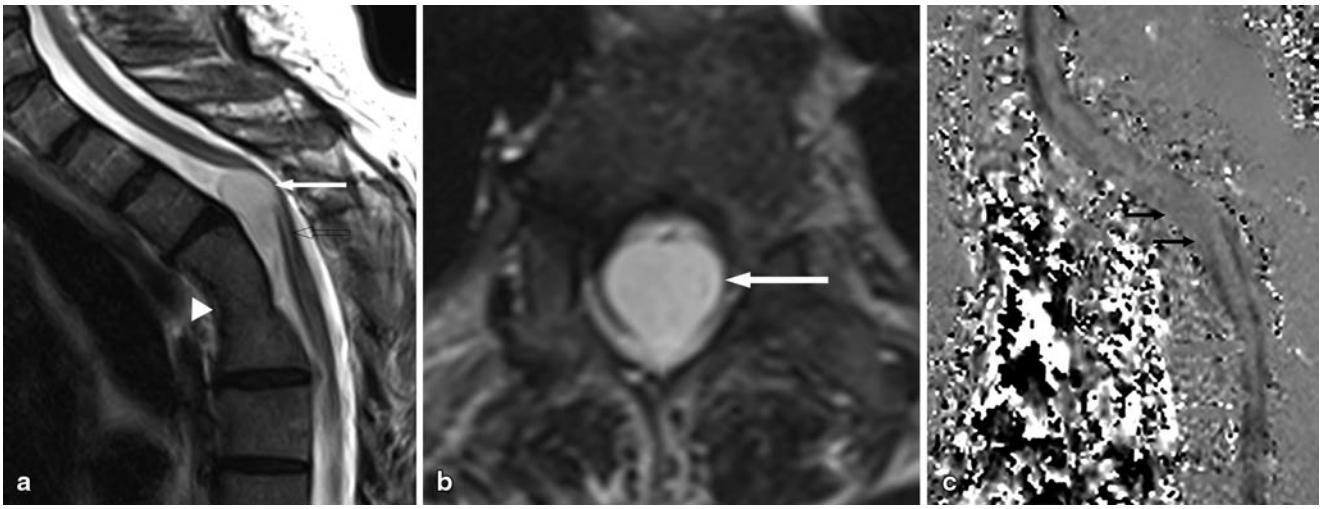

Fig. 7 A 52-year-old man with a neurenteric cyst. Sagittal (**a**) and axial (**b**) T2W image show a vertebral fusion anomaly at T3/T4 (*arrowhead*). An intradural extramedullary cystic lesion (*white arrow*) is seen ventral to the spinal cord at T2/3, causing marked compression and flattening of the spinal cord. An associated syrinx is seen from T1 to T10 (*open arrow*). **c** Phase-contrast MRI demonstrates interrupted flow signal at the level of the cystic lesion (*black arrows*). See Movie 9 for corresponding cine bSSFP sequence.

gests an alternative diagnosis such as asymmetric ventricles or unilateral hydrocephalus, which may be due to ventricular obstruction or CSF overproduction.

Chiari Malformation: Preoperative and Postoperative Evaluation

Chiari I malformation includes the caudal displacement of the cerebellar tonsils below the foramen magnum, and may or may not be associated with a syrinx [32]. As the cerebellar tonsils descend through the foramen magnum, this may cause obstruction of CSF flow around the spinal cord at the foramen magnum (Fig. 8; Movie 10). The degree of tonsillar descent does not predict the severity of symptoms; 14–30 % of patients with greater than 5 mm of tonsillar descent are asymptomatic [33, 34].

Phase-contrast cine MRI is commonly used in the preoperative evaluation of patients with Chiari I for consideration of posterior fossa decompression. Several studies have demonstrated that abnormal CSF flow at the foramen magnum demonstrated on preoperative MRI correlated with postoperative resolution of symptoms [35–37]. Conversely, in patients with normal flow on phase-contrast MRI preoperatively, surgery was more likely to fail to provide symptomatic relief. The degree of obstruction on phase-contrast MRI is a better predictor of postsurgical outcome than the degree of tonsillar descent [35, 36].

Cine bSSFP can provide additional information by visualizing the posterior fossa structures during the cardiac cycle. Preoperatively, this allows dynamic assessment of tonsillar descent through the foramen magnum, and the degree of impaction of the medulla on the dens with each heartbeat.

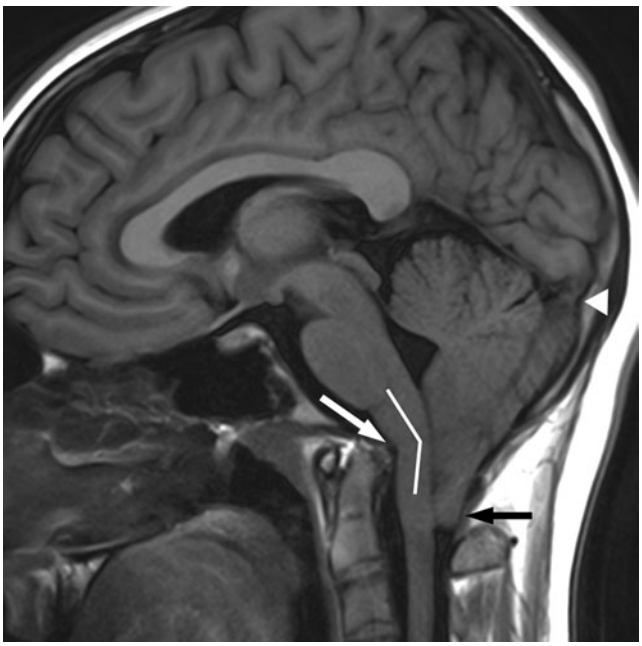

Fig. 8 A 17-year-old girl with Chiari I malformation. Sagittal T1W image demonstrates typical features of Chiari I malformation. The posterior fossa is small with low position of the torcula (*white arrowhead*) and obex. The peg-shaped cerebellar tonsils herniate 2.4 cm below foramen magnum (*black arrow*). The dens is retroflexed (*white arrow*) and indents the medulla, which demonstrates a "bowstring" deformity (*white line*). See Movie 10 for corresponding cine bSSFP sequence.

This provides additional information to phase-contrast MRI in selecting patients who will more likely have symptomatic response following posterior fossa decompression (Fig. 9; Movies 11 and 12).

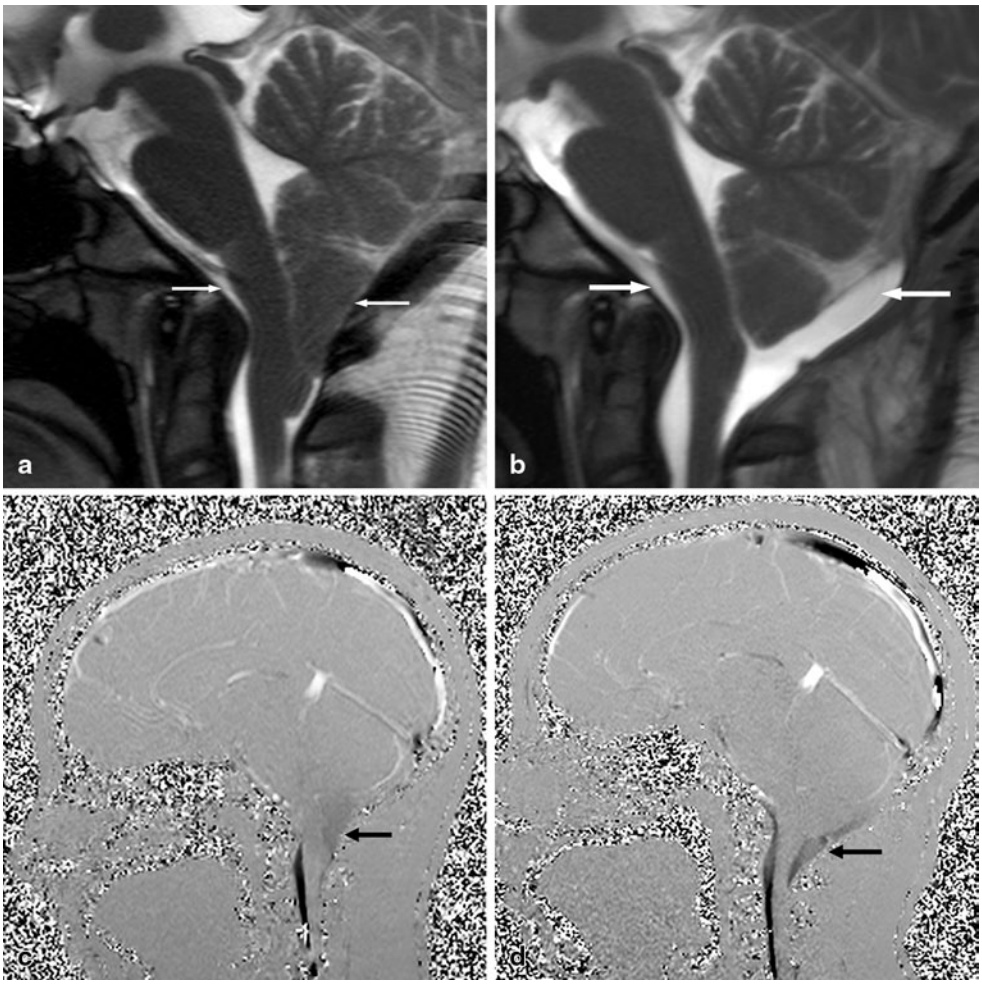

Fig. 9 Symptomatic 14-year-old girl with Chiari I malformation, who underwent posterior fossa decompression surgery. **a** Preoperative still image from cine bSSFP sequence shows typical features of Chiari I malformation. There is effacement of the subarachnoid space at the foramen magnum (*white arrows*). **b** Postoperative still bSSFP image in the same patient following posterior fossa decompression shows that the anterior and posterior spaces at the cervicomedullary junction are larger (*white arrows*). **c** Preoperative and **d** postoperative phase-contrast MRI demonstrate greatly improved postoperative flow inferior to the cerebellum (*black arrows*). See Movies 11 and 12 for corresponding cine bSSFP sequences.

The goals of decompression surgery for Chiari I malformations are to enlarge the volume of the posterior fossa, decompress the inferior cerebellum, and re-establish CSF flow through the foramen magnum [38]. Various surgical techniques have been used to achieve this. Commonly used approaches include osseous decompression, with or without dural grafting, intradural dissection of adhesions, and resection of the cerebellar tonsils [39].

Postoperatively, cine bSSFP allows dynamic visualization of the movement of the posterior fossa structures, rather than relying on assumptions based on CSF flow as in phase-contrast MRI. Postsurgical complications such as adhesions can be diagnosed on bSSFP by detection of a fine hypointense arachnoid band tethering the cerebellum or cervical cord to the cranium or the duraplasty or tethering of the dorsal cerebellar surface to the overlying dural graft (Fig. 10; Movies 13 and 14).

Miscellaneous

Other proposed clinical applications for bSSFP include the evaluation of cerebral aqueduct stenosis and postoperative evaluation of third ventriculostomy and anatomic studies of arachnoid membranes such as the Liliequist membrane [3]. Cine bSSFP can also delineate the septations in a syrinx, which are often too fine to resolve on conventional T2W sequences (Fig. 11; Movie 15). Another potential application of cine bSSFP is the diagnosis of tethered cord syndrome, allowing comparison of spinal cord motion in pre- and post-surgical settings. Constructive interference in steady-state (CISS) MRI techniques have been reported to allow visualization of the tethered filum terminale [40]. CISS MRI has also been used to demonstrate the cyst wall and scolex in cases of intraventricular neurocysticercosis [41], and this may be another potential application of cine bSSFP MRI.

Pitfalls and Artifacts

The main artifact with cine bSSFP is the presence of banding artifact, which commonly occurs in the thoracic spine [1]. This occurs as bSSFP is susceptible to artifacts from magnetic field inhomogeneities. Banding artifacts appear as thick linear hypointensities that are usually fixed during

Fig. 10 A 50-year-old woman who had multiple posterior fossa decompressions for Chiari I malformation. Sagittal T2W image shows pseudomeningocele inferior to the cerebellar vermis (*white arrows*). A small cervical syrinx is present (*open arrow*). See Movies 13 and 14 for corresponding cine bSSFP sequences.

the cardiac cycle. Rephasing with gradients does not reverse the effects of extrinsic inhomogeneities as in fast spin echo sequences, which utilize a 180° RF pulse. Therefore, the decay is more representative of T2* imaging than T2. Dark band artifacts are seen at sites of inhomogeneity in the main magnetic field [42]. These often occur at air–tissue interfaces or at the periphery of the shim field [43, 44].

Several techniques can be used to overcome banding artifacts, including shimming, which uses magnetic field gradients to correct minor magnetic field inhomogeneities [16, 45]. The center of the shim field should be positioned in the study region of interest, for example, the region of suspected arachnoid membranes or CSF flow blockage (Fig. 12; Movies 16 and 17). The field of view should be kept as small as possible. The TR should be kept short to a few milliseconds to improve off-resonance frequency coverage [4, 16, 45]. The phase-encoding direction should be chosen so that aortic or cardiac motion is not superimposed on the region of interest [1].

If banding artifacts cannot be eliminated, these bands may still be differentiated from arachnoid membranes and cyst walls. Banding artifacts tend to be thick and fixed throughout the cardiac cycle, whereas arachnoid membranes are usually thinner and move with CSF pulsations [1].

Another limitation of bSSFP is that only one slice is acquired at a time, rather than a stack or volume. This can be overcome by acquiring slices in different planes, although this can be time consuming. The selection of a single slice of imaging is also operator dependent.

Conclusions

Cine bSSFP is a cardiac-gated MRI technique that provides high contrast and spatial resolution, and is well suited for

Fig. 11 A 44-year-old woman with Chiari I malformation and large cervicothoracic syrinx, with a history of previous posterior fossa decompression. **a** Sagittal T2W image shows cervicothoracic syrinx expanding the cord, with effacement of the spinal subarachnoid space. CSF flow artifact is seen in the syrinx cavity (*black arrows*). There is congenital fusion of the C2 and C3 vertebral bodies. **b** Corresponding still frame from cine bSSFP MRI shows fine septations within syrinx (*arrows*). **c** Sagittal T2W image 5 months following repeat posterior fossa decompression shows marked reduction in size of the syrinx. See Movie 15 for corresponding cine bSSFP sequence.

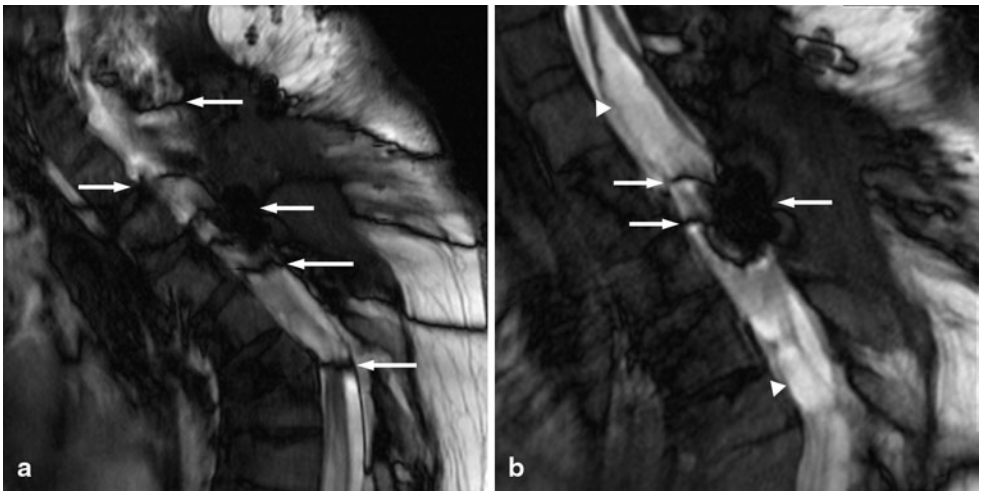

Fig. 12 Example of banding artifact. **a** Several thick band artifacts (*white arrows*) are seen obscuring the region of interest. **b** The field of view is repositioned to reduce the banding artifact and allow better visualization of the thoracic syrinx (*arrowhead*). Some banding artifact is still present (*white arrows*). See Movies 16 and 17 for corresponding cine bSSFP sequences.

the evaluation of the dynamic movement of the neural structures in the subarachnoid space with each heartbeat. This technique facilitates the diagnosis of intraspinal or intracranial arachnoid cysts, evaluation of idiopathic syringomyelia, lateral ventricular asymmetry, and in the preoperative and postoperative assessment of Chiari I malformation, particularly as an adjunct to the more widely used phase-contrast cine MRI. The main limitation of cine bSSFP MRI is the presence of banding artifacts, which can be minimized with various techniques.

Conflict of Interest No grant funding or financial support was received by any author for the creation of this work. The authors have no conflict of interest with the material presented in this article.

Movie Legends

Movie 1 Cine bSSFP sequence. Normal brain motion is pulsatile, with caudal movement of the brainstem and cerebellar tonsils during systole, with return to neutral position in diastole

Movie 2 Cine bSSFP sequence demonstrates a fine arachnoid membrane posterior to the spinal cord at the lower level of the syrinx at T4/5

Movie 3 Intraoperative video demonstrates the presence of an arachnoid band dorsal to the spinal cord. Microneurosurgical lysis of the arachnoid band is performed

Movie 4 Sagittal cine bSSFP sequence clearly demonstrates superior wall of arachnoid cyst and associated mass effect on the spinal cord

Movie 5 Cine phase-contrast scan demonstrates turbulent flow at the superior margin of the arachnoid cyst

Movie 6 Cine bSSFP shows the superior and inferior cyst walls. Further compression of the spinal cord is seen with each heartbeat

Movie 7 Sagittal cine bSSFP: the cyst walls are more clearly appreciated with dynamic imaging

Movie 8 Coronal cine bSSFP: the cyst walls are more clearly appreciated with dynamic imaging

Movie 9 Sagittal cine bSSFP shows more clearly the cyst walls, with exaggeration of the mass effect on the spinal cord seen each heartbeat

Movie 10 Cine bSSFP sequence shows that with each heartbeat, there is downward displacement of the brainstem exacerbating ventral compression of the medulla. Tonsillar impaction on the dorsal dura is also seen

Movie 11 Impaction of the medulla on the dens is seen with exaggerated tonsillar motion. There is effacement of the subarachnoid spaces at the foramen magnum

Movie 12 Following posterior fossa decompression, mass effect on the medulla has decreased

Movie 13 Sagittal cine bSSFP sequence demonstrates dorsal tethering of the medulla, inferior cerebellar vermis, and upper cervical cord due to adhesions. There is loss of normal pulsatile motion at the cervicomedullary junction

Movie 14 Cine bSSFP following repeat posterior fossa decompression and adhesiolysis. Subtle motion of the upper spinal cord is now seen

Movie 15 Corresponding cine bSSFP shows fine septations within syrinx

Movie 16 Sagittal cine bSSFP sequence shows several thick band artifacts obscuring the thoracic cord syrinx

Movie 17 The field of view is repositioned to reduce the banding artifact and allow better visualization of the thoracic syrinx. Some banding artifacts are still present

References

1. Gottschalk A, Schmitz B, Mauer UM, Bornstedt A, Steinhoff S, Danz B, Schlötzer W, Rasche V. Dynamic visualization of arachnoid adhesions in a patient with idiopathic syringomyelia using high-resolution cine magnetic resonance imaging at 3T. J Magn Reson Imaging. 2010;32:218–22.
2. Cousins J, Haughton V. Motion of the cerebellar tonsils in the foramen magnum during the cardiac cycle. AJNR Am J Neuroradiol. 2009;30:1587–8.
3. Reubelt D, Small LC, Hoffmann MHK, Kapapa T, Schmitz BL. MR imaging and quantification of the movement of the lamina terminalis depending on the CSF dynamics. AJNR Am J Neuroradiol. 2009;30:199–202.
4. Chavhan GB, Babyn PS, Jankharia BG, Cheng H-LM, Shroff MM. Steady-state MR imaging sequences: physics, classification, and clinical applications. Radiographics. 2008;28:1147–60.
5. Colaiacomo MC, Masselli G, Polettini E, Lanciotti S, Casciani E, Bertini L, Gualdi G. Dynamic MR imaging of the pelvic floor: a pictorial review. Radiographics. 2009;29:e35.
6. Courtier J, Ohliger M, Rhee SJ, Terreblanche O, Heyman MB, MacKenzie JD. Shooting a moving target: use of real-time cine magnetic resonance imaging in assessment of the small bowel. J Pediatr Gastroenterol Nutr. 2013;57:426–31.
7. Poncelet BP, Wedeen VJ, Weisskoff RM, Cohen MS. Brain parenchyma motion: measurement with cine echo-planar MR imaging. Radiology. 1992;185:645–51.
8. Mokri B. The Monro-Kellie hypothesis: applications in CSF volume depletion. Neurology. 2001;56:1746–8.
9. Enzmann DR, Pelc NJ. Brain motion: measurement with phase-contrast MR imaging. Radiology. 1992;185:653–60.
10. Greitz D, Wirestam R, Franck A, Nordell B, Thomsen C, Stahlberg F. Pulsatile brain movement and associated hydrodynamics studied by magnetic resonance phase imaging. The Monro–Kellie doctrine revisited. Neuroradiology. 1992;34:370–80.
11. Feinberg DA, Mark AS. Human brain motion and cerebrospinal fluid circulation demonstrated with MR velocity imaging. Radiology. 1987;163:793–9.
12. Bieri O, Scheffler K. Fundamentals of balanced steady state free precession MRI. J Magn Reson Imaging. 2013;38:2–11.
13. Carr JC, Simonetti O, Bundy J, Li D, Pereles S, Finn JP. Cine MR angiography of the heart with segmented true fast imaging with steady-state precession. Radiology. 2001;219:828–34.
14. Haacke EM, Wielopolski PA, Tkach JA, Modic MT. Steady-state free precession imaging in the presence of motion: application for improved visualization of the cerebrospinal fluid. Radiology. 1990;175:545–52.
15. Zur Y, Wood ML, Neuringer LJ. Motion-insensitive, steady-state free precession imaging. Magn Reson Med. 1990;16:444–59.
16. Ridgway JP. Cardiovascular magnetic resonance physics for clinicians: part I. J Cardiovasc Magn Reson. 2010;12:71.
17. Klekamp J. Treatment of syringomyelia related to nontraumatic arachnoid pathologies of the spinal canal. Neurosurgery. 2013;72:376–89. Discussion 389.
18. Mauer UM, Freude G, Danz B, Kunz U. Cardiac-gated phase-contrast magnetic resonance imaging of cerebrospinal fluid flow in the diagnosis of idiopathic syringomyelia. Neurosurgery. 2008;63:1139–44. Discussion 1144.
19. Perret G, Green D, Keller J. Diagnosis and treatment of intradural arachnoid cysts of the thoracic spine. Radiology. 1962;79:425–9.
20. Krings T, Lukas R, Reul J, Spetzger U, Reinges MH, Gilsbach JM, Thron A. Diagnostic and therapeutic management of spinal arachnoid cysts. Acta Neurochir. 2001;143:227–34. Discussion 234–5.
21. Kendall BE, Valentine AR, Keis B. Spinal arachnoid cysts: clinical and radiological correlation with prognosis. Neuroradiology. 1982;22:225–34.
22. Silbergleit R, Brunberg JA, Patel SC, Mehta BA, Aravapalli SR. Imaging of spinal intradural arachnoid cysts: MRI, myelography and CT. Neuroradiology. 1998;40:664–8.
23. Mallucci CL, Stacey RJ, Miles JB, Williams B. Idiopathic syringomyelia and the importance of occult arachnoid webs, pouches and cysts. Br J Neurosurg. 1997;11:306–9.
24. Shimizu H, Tominaga T, Takahashi A, Yoshimoto T. Cine magnetic resonance imaging of spinal intradural arachnoid cysts. Neurosurgery. 1997;41:95–100.
25. Yildiz H, Erdogan C, Yalcin R, Yazici Z, Hakyemez B, Parlak M, Tuncel E. Evaluation of communication between intracranial arachnoid cysts and cisterns with phase-contrast cine MR imaging. AJNR Am J Neuroradiol. 2005;26:145–51.
26. Kaufmann HH. Cerebrospinal fluid collections. 1st ed. Thieme, 1998.
27. Osborn AG, Preece MT. Intracranial cysts: radiologic-pathologic correlation and imaging approach. Radiology. 2006;239:650–64.
28. Maiuri F, Iaconetta G, Gangemi M. Arachnoid cyst of the lateral ventricle. Surg Neurol. 1997;48:401–4.
29. Park SW, Yoon SH, Cho KH, Shin YS. A large arachnoid cyst of the lateral ventricle extending from the supracerebellar cistern—case report. Surg Neurol. 2006;65:611–4.
30. Yeates A, Enzmann D. An intraventricular arachnoid cyst. J Comput Assist Tomogr. 1979;3:697–700.
31. Nakase H, Hisanaga M, Hashimoto S, Imanishi M, Utsumi S. Intraventricular arachnoid cyst. Report of two cases. J Neurosurg. 1988;68:482–6.
32. Alden TD, Ojemann JG, Park TS. Surgical treatment of Chiari I malformation: indications and approaches. Neurosurg Focus. 2001;11:E2.
33. Meadows J, Kraut M, Guarnieri M, Haroun RI, Carson BS. Asymptomatic Chiari type I malformations identified on magnetic resonance imaging. J Neurosurg. 2000;92:920–6.
34. Elster AD, Chen MY. Chiari I malformations: clinical and radiologic reappraisal. Radiology. 1992;183:347–53.
35. Ventureyra ECG, Aziz HA, Vassilyadi M. The role of cine flow MRI in children with Chiari I malformation. Childs Nerv Syst. 2003;19:109–13.
36. McGirt MJ, Nimjee SM, Fuchs HE, George TM. Relationship of cine phase-contrast magnetic resonance imaging with outcome after decompression for Chiari I malformations. Neurosurgery. 2006;59:140–6. Discussion 140–6.
37. Armonda RA, Citrin CM, Foley KT, Ellenbogen RG. Quantitative cine-mode magnetic resonance imaging of Chiari I malformations: an analysis of cerebrospinal fluid dynamics. Neurosurgery. 1994;35:214–23. Discussion 223–4.
38. Mazzola CA, Fried AH. Revision surgery for Chiari malformation decompression. Neurosurg Focus. 2003;15:E3.
39. Haroun RI, Guarnieri M, Meadow JJ, Kraut M, Carson BS. Current opinions for the treatment of syringomyelia and chiari malformations: survey of the Pediatric Section of the American Association of Neurological Surgeons. Pediatr Neurosurg. 2000;33:311–7.

40. Rosahl SK, Kassem O, Piepgras U, Hellwig D, Samii M. High-resolution constructive interference in steady-state imaging in tethered cord syndrome: technical note. Surg Neurol. 2005;63:372–4.
41. Govindappa SS, Narayanan JP, Krishnamoorthy VM, Shastry CH, Balasubramaniam A, Krishna SS. Improved detection of intraventricular cysticercal cysts with the use of three-dimensional constructive interference in steady state MR sequences. AJNR Am J Neuroradiol. 2000;21:679–84.
42. Baskaran V, Pereles FS, Russell EJ, Georganos SA, Shaibani A, Spero KA, Krupinski EA, Zhang A, Finn JP. Myelographic MR imaging of the cervical spine with a 3D true fast imaging with steady-state precession technique: initial experience. Radiology. 2003;227:585–92.
43. Absil J, Denolin V, Metens T. Fat attenuation using a dual steady-state balanced-SSFP sequence with periodically variable flip angles. Magn Reson Med. 2006;55:343–51.
44. Finn JP, Nael K, Deshpande V, Ratib O, Laub G. Cardiac MR imaging: state of the technology. Radiology. 2006;241:338–54.
45. Lee J, Lustig M, Kim DH, Pauly JM. Improved shim method based on the minimization of the maximum off-resonance frequency for balanced steady-state free precession (bSSFP). Magn Reson Med. 2009;61:1500–6.